C. R. Mecanique 345 (2017) 66–77

Contents lists available at ScienceDirect

Comptes Rendus Mecanique

www.sciencedirect.com

Basic and applied researches in microgravity/Recherches fondamentales et appliquées en microgravité

On the interest of microgravity experimentation for studying convective effects during the directional solidification of metal alloys

Henri Nguyen-Thi *, Guillaume Reinhart, Bernard Billia

Aix Marseille Université, CNRS, IM2NP UMR 7334, Campus Saint-Jérôme, case 142, 13397 Marseille, France

ARTICLE INFO

Article history:
Received 18 March 2016
Accepted 2 September 2016
Available online 15 November 2016

Keywords:
Directional solidification
Microstructures
Convection
Microgravity
In situ characterization
Metallic alloys

ABSTRACT

Under terrestrial conditions, solidification processes are often affected by gravity effects, which can significantly influence the final characteristics of the grown solid. The low-gravity environment of space offers a unique and efficient way to eliminate these effects, providing valuable benchmark data for the validation of models and numerical simulations. Moreover, a comparative study of solidification experiments on earth and in low-gravity conditions can significantly enlighten gravity effects. The aim of this paper is to give a survey of solidification experiments conducted in low-gravity environment on metal alloys, with advanced post-mortem analysis and eventually by in situ and real-time characterization.

1. Introduction

Structural material properties are directly related to their solidification microstructures, so that a precise control of the growth process is crucial in engineering [1]. Depending on the applied processing parameters and on the material physical parameters, a wide variety of solidified microstructures are observed in casting, in welding, and in other solidification processes. The most common structure is dendrite, which can be either equiaxed, when solidification occurs in nearly isothermal conditions like in the case of a snowflake, or columnar in the presence of a temperature gradient. Depending on the application, one type of grain structure is preferred and thus favored, e.g., equiaxed grains in car engines and columnar grains in turbine blades. These patterns can be described by suitable length scales such as dendritic primary spacing and tip radius. In pure diffusive transport regime, characteristic laws have been proposed to relate those shape characteristics to processing conditions. However, for most real solidification processes, and especially at low growth rate, gravity effects such as natural convection, sedimentation/buoyancy, mechanical effects and change in hydrostatic pressure cannot be neglected and significantly affect morphological instability [2]. The coupling between gravity effects and solidification has been the subject of a great deal of experimental, theoretical and numerical works since the birth of microgravity experimentation in the early eighties. The main conclusion of all these studies is that gravity is the major source of various disturbing effects, which can significantly modify or mask important physical mechanisms on Earth ($1g$). A review of some effects induced by gravity on the solidification process and investigated by mean of synchrotron X-ray radiography at the ESRF (European

* Corresponding author.
E-mail address: henri.nguyen-thi@im2np.fr (H. Nguyen-Thi).

http://dx.doi.org/10.1016/j.crme.2016.10.007

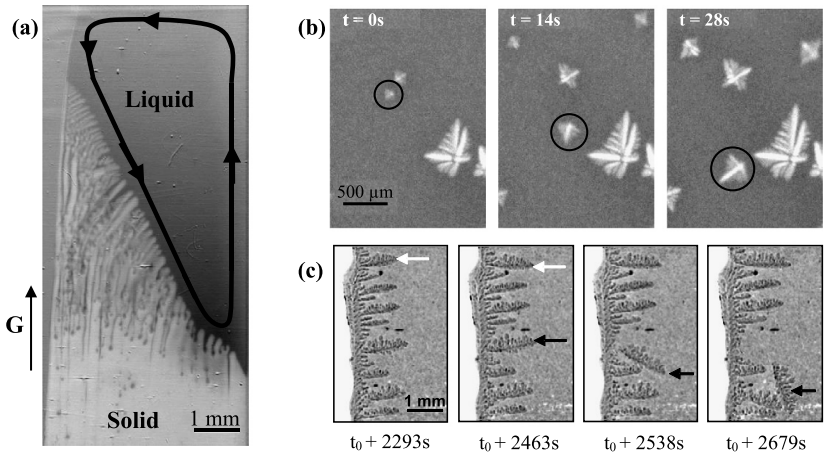

Fig. 1. In situ observation of gravity effects during direction solidification. (a) Deformation of the solid–liquid interface due to a convection loop forming during directional solidification of Al–4wt.%Cu (cooling rate = 0.3 K/min, temperature gradient = 35.5 K/cm). (b) Sequence of radiographs recorded during Al–10wt.%Cu equiaxed solidification showing the sedimentation of equiaxed grains. (c) Radiographs showing the bending and the fragmentation of secondary arms during the development of a columnar dendrite of Al–7wt.%Si (cooling rate = 0.5 K/min, temperature gradient = 15 K/cm).

Synchrotron Radiation Facility) in thin aluminum-based alloys is presented elsewhere [2], namely convection effects on the solid–liquid interface during the initial transient of solidification [3] (Fig. 1a), the sedimentation or floatation of equiaxed grains (Fig. 1b), and its effect on the columnar-to-equiaxed transition [4,5], and finally the cumulative mechanical moments induced by gravity on the dendrite during solidification [6,7], leading to the bending of the secondary arm of the dendrite (Fig. 1c).

Numerous experiments in microgravity conditions have shown that microgravity (µg) environment is a unique and efficient way to eliminate buoyancy and convection to provide benchmark data for the validation of models and numerical simulations. For these reasons, materials science and more particularly solidification of metal alloys has been a prominent topic of research in the microgravity field, since the early stages of microgravity experimentation. In a microgravity environment, transport phenomena are essentially diffusive and buoyancy forces vanish, which highly simplifies the experiment's analysis and allow a more direct and precise comparison with theoretical models [8]. Let us mention here the outstanding experiment IDGE (Isothermal Dendritic Growth Experiment), performed in low-earth orbit by M.E. Glicksman and co-workers [9–13]. The IDGE was developed specifically to test dendritic growth theories by performing measurements with succinonitrile (SCN) and pivalic acid (PVA) under strictly diffusion-controlled conditions. The IDGE instrument was flown three times aboard the space shuttle Columbia, as part of NASA's missions, from 1994 to 1997 [12]. This series of experiments (hundreds of repeated experiments of steady-state dendritic growth) provided the first solid evidence that dendritic growth is indeed governed by heat diffusion from the solid–liquid interface. However, experiments also showed that Ivantsov's solution describing the diffusion process for a paraboloid crystal tip requires some modifications. The tip velocity and tip radius data were measured as functions of the initial undercooling and Glicksman's analysis indicated that, at least for pure SCN, the average scaling factor $\sigma^* \sim 0.02$ is a value that is independent of both undercooling and gravitational environment. The robustness of the interfacial scaling law, namely $V R^2 = \text{constant}$, where V is the velocity of the tip and R is the curvature radius at the tip, appears to be independent of the gravity environment, with a slight dependence on undercooling.

In addition, comparative studies of solidification experiments in 1g and µg can also enlighten the effects of gravity. A demonstrative example of such a study on this topic is the work performed by M.D. Dupouy, D. Camel and J.-J. Favier in the early 1990s by post-mortem analysis of Al–Cu samples solidified during the D1 – Spacelab mission [14–16]. Low-concentration (1wt%) hypo- and hyper-eutectic alloys (26wt% and 40wt%) were directionally solidified under a temperature gradient of 25 K/cm. The influence of gravity on the structural transitions (dendritic/eutectic and cell-dendrite transitions), the difference between the space and ground samples primary spacing and the dendritic array morphology were thoroughly analyzed, showing a strong impact of the transport mode in the melt. In particular, the primary arm spacing was found five times larger in space than on Earth [14–16].

The results presented in this article are a selection of microgravity solidification experiments carried out by our team onboard two platforms (American shuttle and sounding rocket) on aluminum-based alloys. For each experiment, we first briefly describe the scientific objectives, the apparatus and the experimental procedure. Then we present the most significant results obtained in the framework of the experiments conducted in gravity-reduced conditions, and the effects of gravity-free conditions will be enlightened. We omitted in this review the recent experiments performed on the International Space Station on transparent alloys [17,18] or on Al–Si alloys [19,20], whose detailed analysis is still ongoing and would deserve a longer paper.

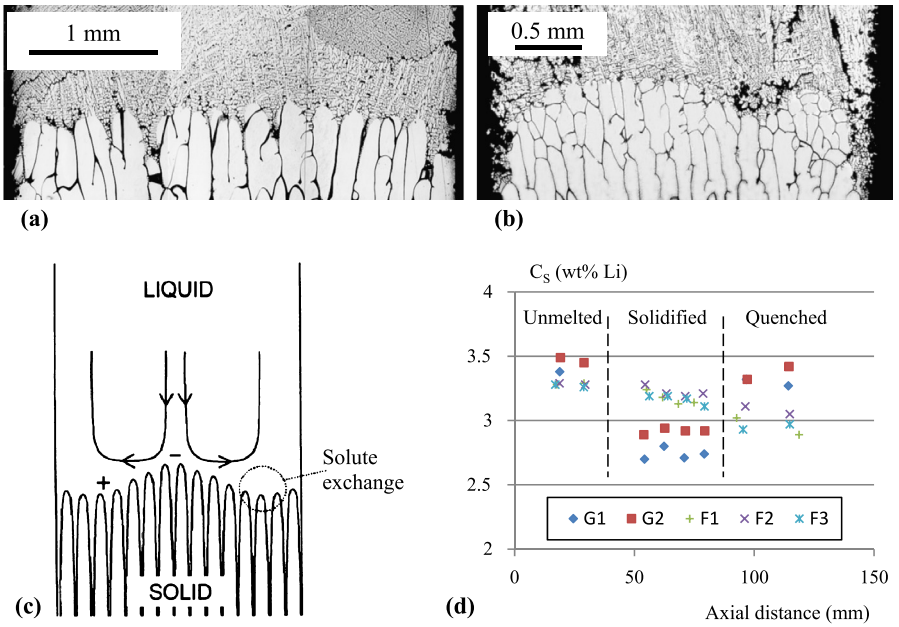

Fig. 2. (a) and (b): Longitudinal sections showing the macroscopic shapes of the quenched solid–liquid interface of samples processed in microgravity (F2) and on the ground (G2). (c) Schematic representation of convective flow (boundary layer mode). (d) Axial composition profile for flight (open symbols) and ground (full symbols) samples.

2. Influence of solutal convection on the solidification of Al–3.5wt%Li alloy

For most real solidification processes, in particular at low growth rate, natural convection and its influence on the grain structure or the solid–liquid microstructure cannot be neglected [21–23]. On Earth, natural convection or fluid flow is induced by built-in constitutional and thermal gradients in the liquid phase. In practice, solutal convection dominates in the case of metallic alloys owing to their large Lewis number defined as the ratio of the thermal diffusivity to the solutal one ($Le = D_{\mathrm{th}}/D$), typically of the order of 10^3 to 10^4. The coupled convective–morphological instability may be separated in two distinct regions: within the mushy layer (generally considered as a porous medium) and a boundary layer ahead of the mush/liquid interface. In the latter case, the characteristic length scale may vary from several dozen times the solutal length D/V, with V the solidification velocity (convection in a buffer region), up to the sample size (bulk convection), depending on the alloys (partition coefficient k and respective densities of liquid and solid phases) and the experimental conditions (in particular growth direction versus gravity). The complexity of the topic was the major reason to carry out solidification experiments in convection-free conditions, when thermal and solutal transports are essentially diffusive [8]. The obtained results can be then used as quantitative reference/benchmark data to validate theories or numerical simulations.

2.1. Microgravity experiments during the D2 mission

For this purpose, solidification experiments were performed on Al–3.5wt%Li in the Bridgman apparatus GFQ (Gradient Furnace with Quenching) in both normal and microgravity conditions. For ground experiments, alloys were solidified vertically upward to obtain a solutal destabilizing configuration. Indeed, during the growth process, the rejected solute (Li) is lighter than the solvent (Al), which yields that both interstitial fluid and solute boundary layer are unstably stratified and that buoyancy-driven convection in both zones is unavoidable. Three microgravity experiments (labeled F1, F2 and F3) were performed onboard the American space shuttle *Columbia* during the German spacelab mission D2 in 1993, with a temperature gradient close to 70 K/cm and pulling rates of 6.3, 7.2 and 12.2 μm/s [24,25]. These experiments were compared to two ground samples (labeled G1 and G2) carried out in the same apparatus and for nearly the same experimental parameters ($G = 70$ K/cm and $V = 5.6$ and 9.3 μm/s).

2.2. Effects of natural convection on macroscopic scale characteristics

The quenched solid–liquid interfaces were revealed by metallographic analysis of longitudinal section of the solidified samples. As expected, the solid–liquid interfaces for μg samples are nearly flat (Fig. 2a), whereas they are modulated at the macroscopic scale for samples grown vertically upward on the ground (Fig. 2b). The macroscopic modulation of the growth front is the footprint of the thermo-solutal convective rolls as explained by Nguyen-Thi et al. [26] for the solidification of Pb–30wt%Tl and represented in Fig. 2c: below an upwelling current, there is an excess of solute thus creating a trough,

whereas below a downwelling current bringing less rich fluid there is a depletion of solute, thus creating a crest. Note that exchange of solute between the region ahead of the front and the bulk liquid must occur to account for the measured axial macrosegregation.

Indeed, the axial composition profiles obtained by chemical analysis of thin slices along the samples show a larger deviation from the ideal diffusive case for ground samples than for μg samples (Fig. 2d). For μg samples, the composition profiles continuously decreased along the sample, probably due to a progressive loss of lithium during the course of the experiments that were performed under vacuum. For ground samples, sharp variations were found at the beginning of the solidification (from 3.5wt.% to 2.7wt.% for G1 and 2.9wt.% for G2) and after quenching (up to 3.3wt.% for both ground samples), which testifies to the occurrence of axial macrosegregation. In addition, it has been possible to estimate the values of the effective partition coefficient $k_{\text{eff}} = C_S/C_\infty$, where C_∞ is the bulk liquid composition, assumed equal to that of the quenched liquid, and C_S is the solid composition measured during steady-state solidification and assumed to be equal to the composition of the solid just before the quench. The values of k_{eff}, deduced from the axial macrosegregation measurement in Fig. 2d, were close to unity for microgravity experiments, as expected in essentially diffusive transport conditions, while they are about 0.83 ± 0.03 for G1 and 0.88 ± 0.03 for G2, which are between the equilibrium partition coefficient $k = 0.55$ and unity [27]. This confirmed a partial mixing of the bulk liquid by convection during solidification. It can be also noted that, for this type of convection, despite the curvature of the front, the radial segregation is not strong, due to the fluid flow along the solid–liquid interface [25,26]. In conclusion, the solid–liquid interface is macroscopically planar, with neither radial nor axial macrosegregation only during the solidification performed in microgravity conditions.

2.3. Primary arm spacing measurements

For all experiments performed, a detailed analysis of several microscopic characteristics was conducted and reported in reference [25]. In this paper, we focus on a key parameter of the cellular/dendritic arrays, namely the average primary spacing λ, which can be easily measured on cross-sections of the solidified samples (Fig. 3a). Like in our previous experiments on Pb–30wt.%Tl alloys [28], we found that, during both their dynamical formation from morphological instability and their asymptotic state, the cell/dendrite arrays could be described by a honeycomb on which a large amount of disorder (displacement of cell centers from their ideal positions) is superimposed. The statistical analysis of such type of image has been described in details elsewhere [29]. In these experiments, average values and standard deviations were calculated for more than 250 cells. By a comparative study of measurements performed on ground and microgravity samples, it has been confirmed that, even in nearly ideal conditions, there is no selection of a unique primary spacing and only an average value can be determined with a large standard deviation (Fig. 3b), typically about 20–30%. The large standard deviation for microgravity samples, identical to ground-based ones, also ruled out the hypothesis that convection is the main cause of the high disorder generally observed in cellular/dendritic pattern in experiments carried out on Earth. The influence of some additional extrinsic effects, namely effect of crucible, grain boundary, gas pores or the experimental procedure, on the dynamics and selection of cellular arrays was also studied [30]. During the solidification of massive transparent samples, it has been established that the main source of disorder in cellular arrays is the front curvature, which induces a collective gliding of the whole cellular array down the interface slope, and the elimination of coarse cells at the central sink [31]. The main conclusion is that the disorder in a cellular/dendritic pattern is intrinsic to the dynamics of the solid–liquid interface.

Mean primary spacings of flight samples are given in Fig. 3c, as a function of the growth rate. Hunt and Lu [32] considered that the minimum stable spacing of a cellular array is the spacing for which the composition along the cell groove is nearest to the liquidus one. From numerical calculations, these authors proposed the following expression:

$$\lambda_{\min} = 8.18\, k^{-0.335} \left(\frac{\Gamma}{m_L C_\infty (k-1)} \right)^{0.41} \left(\frac{D}{V} \right)^{0.59} \tag{1}$$

where Γ is the Gibbs–Thomson coefficient and m_L is the liquidus slope. This equation is plotted in Fig. 3c with $\Gamma = 2 \cdot 10^{-5}$ K · cm (typical order of magnitude for Al-based alloys), $m_L = -8.3$ K/wt%Li [33], $D = 1.9 \cdot 10^{-4}$ cm^2/s, $k = 0.55$, and $C_\infty = 3.32$wt.%Li (mean value for flight samples, see Fig. 2d). The results of Fig. 3c show that in μg conditions the experimental spacing decreases for increasing growth rates, as expected for cells, and is only 10–20%, i.e. less than what is predicted by the model of Hunt and Lu, in particular for the lowest pulling rate, when the influence of natural convection was expected to be more important.

3. Convection caused by radial thermal and solutal gradients

In the previous case (Al–3.5wt%Li), the rejected solute was lighter, so that the liquid configuration was solutally destabilizing in upward solidification on ground. In order to avoid natural convection in the melt, it seems reasonable to ensure that the density gradient is solutally stable, i.e. vertical everywhere and with the heaviest material being at the bottom. This situation is more or less approached when growth takes place upwards in an alloy system in which the rejected (respectively absorbed) solute is denser (respectively lighter) than the solvent. This is the case for Al–1.5wt%Ni, for which almost all the solute (Ni) is rejected during solidification ($k = 0.0087$). Actually, even in this experimental configuration, flow patterns adjacent to the front are known to develop under the effect of any horizontal density gradient, as revealed by the

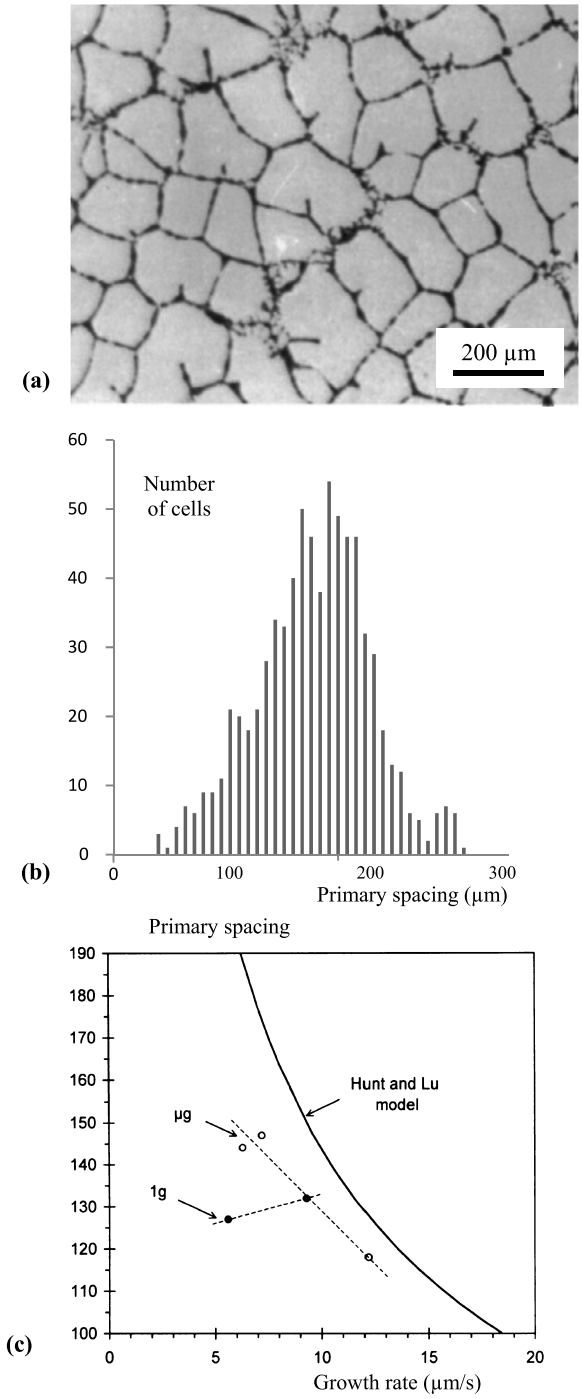

Fig. 3. (a) Cross section of sample F2 in the quenched solid–liquid zone. (b) Histogram of the primary spacing for F2 (about 250 cells) and (c) of the primary spacing as a function of the growth rate for samples processed in microgravity and on the ground; comparison with the Hunt and Lu's model.

macroscopic front deformation and lateral microstructure heterogeneity observed at low solidification rates. A first qualitative evidence of these effects was given in [34], where front shapes were studied as a function of the solidification rate in several Al–Cu alloys solidified above the morphological instability threshold. Since then, similar effects have been observed below this threshold both in transparent [22] and semiconductor systems. In addition, the influence of convection on the dendritic microstructure was demonstrated in [14] by comparing the patterns obtained on Earth with those formed under identical solidification conditions in a microgravity environment. It was in particular found that in such a configuration with

Table 1
Experimental control parameters of the AGHF experiments: FM (Flight Model) for experiments in microgravity conditions and GM (Ground Model) for experiments on Earth.

Sample μg	Thermal gradient (K/cm)	Pulling rate (μm/s)	Sample 1*g*	Thermal gradient (K/cm)	Pulling rate (μm/s)
FM1-1	34	3.83	GM1-1	35	3.83
FM1-2	34	1.83	GM1-2	35	1.79
FM2	34	0.83	GM2	33	1.0
FM3-1	24	2.33	GM3-1	25	2.67
FM3-2	24	1.5	GM3-2	25	1.67

a highly permeable mush, the fluid flow was able to strongly reduce the primary dendrite spacing in the regions where it was locally oriented towards the mush.

3.1. Microgravity experiments

Directional solidification was carried out on Al–1.5wt%Ni alloys in both terrestrial and microgravity conditions in the Advanced Gradient Heating Facility (AGHF) of the European Space Agency (ESA). Microgravity experiments (labeled FM) were conducted during the LMS and STS-95 space missions in the American space shuttle *Columbia* (1996) and *Discovery* (1998), respectively. For ground experiments (labeled GM), samples were solidified vertically upwards in a thermal and solutal stabilizing configuration with respect to convection driven by the axial gradients (Table 1).

3.2. Solute segregation at the macroscopic scale

The longitudinal segregation profile was determined by recording the grey-level variation of the radiograph along the sample axis, which also allowed locating the position of the solidification front at the successive stages of the experiment (i.e. end of stabilization, velocity change if any, and quench). The solute concentration profile was then calibrated both by chemical analysis of thin slices (1 mm thick) cut along the sample, and by EDS (Energy-Dispersive Spectroscopy). These analyses were performed in the unmelted part, the solidification zone and the quenched liquid. The relative influence of convection is derived by comparing the results obtained in microgravity and on ground samples.

For all samples, there was a plateau of almost constant concentration during the solidification phase, equal to the initial concentration Al–1.5wt%Ni, measured in the unmelted part of the sample (Fig. 4a). Before this plateau, a complex profile was detectable, which is the result of the TGZM (Temperature Gradient Zone Melting) phenomenon investigated in details in [33,35]. The concentration variation measured near the quenched front (Fig. 4b) indicated the presence of an Ni-enriched layer, which was the characteristic profile resulting from the solute diffusion occurring both in the liquid ahead the front and in the interdendritic or intercellular liquid [36].

Radial segregations were determined in all samples by EDS on cross-sections just below the quenched solid–liquid interface. For microgravity samples, the radial composition profiles were roughly flat, as expected in solidification experiments with essentially diffusive transport conditions. On the contrary, large radial macrosegregation was found for ground samples, despite the negligible longitudinal macrosegregation. The explanation of this effect is that the solute boundary layer adjacent to the tips is swept by the fluid flow driven by the residual radial temperature gradient, due to the difference in thermal conductivities between the solid and liquid phases and the crucible wall. Accordingly, a part of the heat flux transported along the crucible goes into the solid, thus creating a local inward heat flux that leads to a convex shape of the isotherms and a narrow front depression at the crucible wall. This depression is progressively enhanced by the nickel accumulation on the periphery, until the eutectic concentration is reached (Fig. 5). A stationary state is eventually achieved because the radial-gradient-driven fluid flow is confined in a buffer transported at the front velocity with no mixing with the bulk of the melt, which is the mere reason of the absence of fluid flow effect on longitudinal solute macrosegregation.

3.3. Microstructure localization

To obtain the morphology at the quenched solidification front, a metallographic examination was first performed on a longitudinal section. Then, a slice containing the solid–liquid interface was cut and polished to obtain a sequence of closely spaced transverse sections through the solid–liquid zone. Image analysis techniques [29] were applied on optical micrographs of selected regions in order to determine the histograms of primary spacing. Fig. 6 shows typical longitudinal and cross sections for samples solidified in 1*g* (GM2) conditions and in microgravity (FM2), respectively. The section through the quenched front in Fig. 6a, flatted parallel to the growth, indicates microstructure localization, namely cell/dendrite clustering towards the center accompanied by steepling, i.e. the envelope of the tips is strongly distorted and protrudes markedly into the melt ahead of the eutectic front [34]. As shown in Fig. 6a and Fig. 6c, a thin liquid region is present at the periphery down to the eutectic temperature. Comparatively, no front distortion is observed even at low solidification rates in the microgravity samples: the longitudinal section (Fig. 6b) always shows a macroscopically planar shape of the front envelope, except for the steep but narrow depression at the contact with the crucible, which corresponds to the

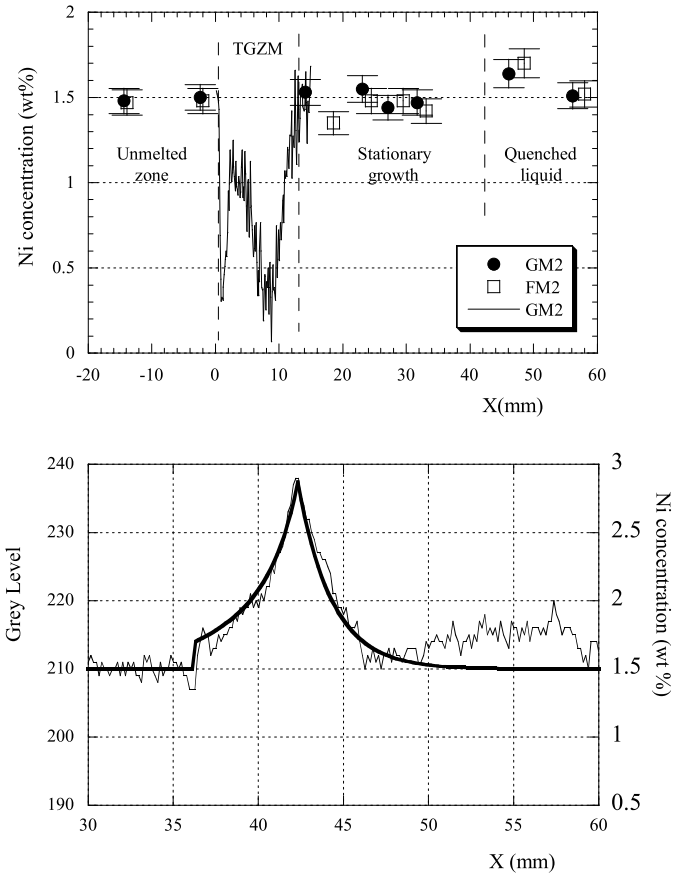

Fig. 4. (a) Profiles of Ni longitudinal macrosegregation in microgravity (FM2) and ground (GM2) samples (chemical analysis of thin slices cut all along the samples), with the variation in the TGZM region superimposed (scan line). (b) Variation of Ni concentration across the quenched mushy zone deduced from the absorption contrast on an X-ray radiograph, and profile predicted by modelling in [36].

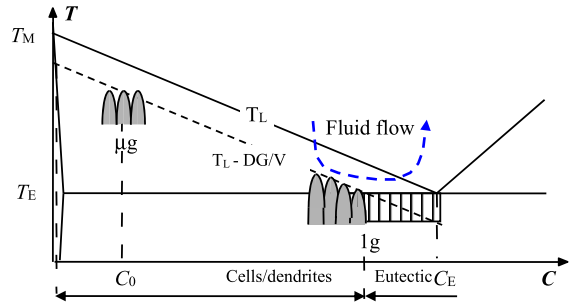

Fig. 5. Sketch of cell/dendrite localization due to radial solute segregation under fluid flow.

region where heat flows from the crucible into the solid. In transverse section (Fig. 6d), a cellular/dendritic microstructure covers the entire surface and no eutectic border is present.

The comparison of ground and microgravity samples definitely demonstrated that convection, created by an initial residual temperature gradient and then amplified by solute rejection, was the cause of the strong macroscopic distortion of the solid–liquid interface. The gradual amplification of convection during the initial transient was analyzed in situ and real-time during the directional solidification of Al–Cu alloys by Bogno et al. [3,37]. Fig. 1a illustrates this effect, showing in two dimensions the steepling and clustering effect. The final depth of the deformation and resulting radial segregation are mainly determined by the amount of solute that can be transported laterally. Moreover, it results from the ground experiments in the AGHF that clustering and steepling effects of buoyancy-driven convection progressively decrease as the solidification velocity is increased, so that diffusive-like dendritic growth is achieved beyond a critical pulling rate [36].

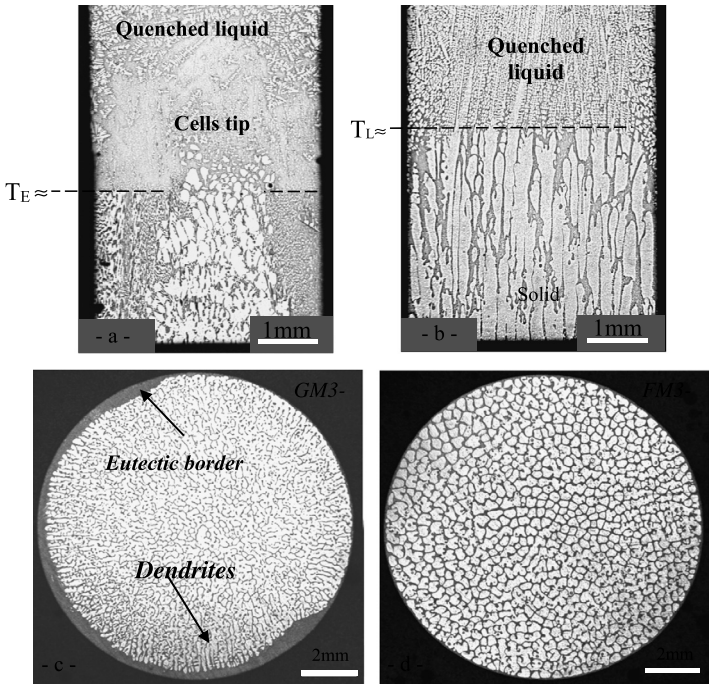

Fig. 6. Comparison of the microstructures obtained during upward solidification on ground (a and c) and in microgravity (b and d) for Al–1.5wt%Ni, $G = 24$ K/cm and $V = 2.3$ μm/s. (a) and (b): Longitudinal sections across the quenched front, (c) and (d) transverse sections below the quenched front.

3.4. Solidification microstructure in the diffusive regime

For the microgravity samples, primary spacings can be measured on the whole transverse sections for a large number of cells. Despite the diffusive conditions, the standard deviation of the primary spacing remains large, about 10–20%. This result is similar to those beforehand described in Al–Li alloys solidified in microgravity conditions [25]. Thus, the present experiments again confirm that, as theoretically emphasized by Ben Amar and Moussalam [38], there is no selection of a unique wavelength during directional solidification. Yet, the average spacing can be determined together with the minimum and maximum spacings (FM3-1: $\lambda_{min} = 190$ μm, $\lambda_{mean} = 378$ μm, $\lambda_{max} = 510$ μm and FM3-2: $\lambda_{min} = 150$ μm, $\lambda_{mean} = 394$ μm, $\lambda_{max} = 600$ μm). The comparison with the numerical predictions of Lu and Hunt's model reveals that the experimental primary spacing is about half of the theoretical value. Up to now, we have no explanation for this large discrepancy.

In relation with the clustering and steepling phenomena caused by convection on ground as discussed before, the ground samples show a radially non-uniform microstructure (Fig. 6a), cellular in the core of the sample and becoming more and more dendritic when approaching the eutectic border at the periphery. Moreover, a strong tendency for these dendrites to grow laterally towards this eutectic region is observed in the region where the local slope of the front of dendrite tips is high (Fig. 6c). This lateral growth is consistent with the fact that the liquid in the depressed liquid region is slightly undercooled due to the horizontal solute gradient. Due to this radial non-uniformity, it is difficult to perform meaningful measurements of primary spacing. Nevertheless, mean primary spacing was estimated for these experiments in the central cellular region where the fluid flow $U_{//}$ is locally directed towards the mush. Thus, the average primary spacings were calculated for a limited number of cells (about 40–50) but the standard deviation $\Delta\lambda$ of the measurements was approximately the same as in the microgravity samples. For each velocity, the average primary spacing measured in ground-based experiments is lower than the one measured in space experiments, similarly to the solidification of Al–Li alloys where the convective configuration was solutally destabilizing [25]. In the present case, this reduction was correlated with the inward direction of the flow using the relationship derived by [14]:

$$\lambda = \frac{\lambda_0}{\sqrt{1 + \frac{U_{//}}{V}}} \tag{2}$$

where λ_0 is the primary spacing measured in space under diffusion transport, $U_{//}$ the velocity of the inward fluid flow and V the solidification velocity. The weaker reduction of primary spacing compared to fully dendritic solidification can then be attributed to the lower flow penetration in a mush of limited permeability, which is reflected by small values of the relative fluid-flow downward velocity $U_{//}/V$ [36].

4. In situ characterization during metal alloy solidification onboard microgravity platforms

As most of the phenomena involved during solidification are dynamical, in situ and real-time observation is mandatory to analyze in details the experiments. Up to now, in situ observation during microgravity solidification experiments were limited to the investigations on transparent organic alloys, using optical methods [39]. However, their behavior is not completely identical to that of metallic systems, in particular due to their low thermal conductivity. Recent developments of more powerful microfocus laboratory X-ray sources, as well as modern X-ray detectors, have led to vast improvements in the performance of X-ray-based techniques. Accordingly, in the frame of ESA-MAP XRMON (in-situ X-ray monitoring of advanced metallurgical processes under micro gravity and terrestrial conditions) project, a novel facility dedicated to the study of the directional solidification of Al-based alloy with in situ X-ray radiography, has been developed. Indeed, X-ray radiography is particularly well suited for in situ studies and is non-destructive to most metallic materials [40]. In this technique, the contrast in the recorded image is due to local changes in the amplitude of the X-ray beam transmitted through the sample. The main objective of this project is to demonstrate the new opportunities X-ray radiography offers in the field of materials science in microgravity [41].

4.1. Brief description of the MASER-12 experiment

The experimental facility consists of a furnace and an X-ray radiography device specifically devoted to the study of Al-based alloys [42]. The gradient furnace is of Bridgman type and special care in the choice of furnace and crucible materials has been taken to provide good X-ray transmission without compromising the thermal properties. The experiment sample is made of Al–20wt.%Cu and is 5 mm in width, 50 mm in length and 150 µm in thickness. The high amount of solute was chosen mainly to ensure a high contrast between the grown solid and the surrounding liquid phase. The imaging system comprises two parts: the X-ray tube and the camera. A microfocus X-ray tube with 3 µm focal spot was used in order to meet a spatial resolution of roughly 5 µm. The X-ray tube was equipped with a thin layer of molybdenum as the transmission target on an aluminum substrate.

The first solidification experiment in microgravity using this facility was successfully carried out during the MASER 12 sounding rocket mission on 13 February 2012. In accordance with the limited microgravity period, a well-adapted experimental timeline had to be precisely defined. After a short stabilization period in microgravity environment, the sample solidification was triggered by applying a cooling rate $R_1 = 0.15$ K/s, to both heaters, at $t = 187$ s. At $t = 400$ s a second cooling rate $R_2 = 0.7$ K/s was applied automatically on both heaters. At last, a few seconds before the end of the microgravity period, the two heaters were switched off and thus the sample naturally cooled down at $R_3 = 5$ K/s, deduced from the thermocouple measurements. Radiographs were successfully recorded during the whole experiment including the melting and solidification phases of the sample, with a field of view of about 5 mm $\times$ 5 mm, a spatial resolution of about 4 µm and a frequency of two frames per second.

The day after the flight, two ground-reference tests were carried out on a fresh sample with the same experimental profile, for two different sample positions. In the first reference test, named 1g-upward experiment, the growth direction was anti-parallel to the gravity vector. In the second reference test, named 1g-horizontal experiment, the sample was in horizontal position with the observation plane perpendicular to the gravity direction. A comparative study was then performed to enable direct comparison between the experiments and therefore to enlighten the effects of gravity upon microstructure formation.

4.2. In situ observation of microgravity experiments

Fig. 7 displays a sequence of images recorded during the solidification of an Al–20wt%Cu alloy in microgravity conditions. This sequence of images shows the time evolution of the interface pattern during the successive cooling rates (0.15 K/s $\rightarrow$ 0.7 K/s $\rightarrow$ natural cool down) and illustrates the great advantage of using X-ray radiography for *in situ* investigation of directional solidification of metallic alloys. In the experiment, the sample was initially fully melted in the Field of View (FoV), so that nucleation of the first solids occurred below the FoV. After a while, dendrite tips appeared in the FOV but only a disordered dendritic pattern could be obtained, due to the nucleation of several grains with different orientations (Fig. 7a). In addition, one can see in Fig. 7b the nucleation of an equiaxed grain ahead of the columnar front (black circle), most likely on a small heterogeneity of the sample oxide layer. This grain slightly rotated, which clearly showed that it was not stuck on the sample walls. However, due to the microgravity environment and the absence of buoyancy, this grain remained at the same altitude and was engulfed by the columnar front (Fig. 7c), and then completely merged into the columnar microstructure (Fig. 7d). At $t = 400$ s, a faster cooling rate was applied on both heaters (0.7 K/s) and a much finer microstructure achieved, which induced a weaker contrast in the radiographs, with a more oriented direction for all dendrites (Fig. 7d). Very close to the end of the solidification, the eutectic front was detected (dashed line in Fig. 7g), allowing us to have an estimate of the length of the mushy zone, typically 5 mm. Fig. 7h shows the final grain structure at the end of the experiment. The grain structure is mainly composed of columnar grains all along the field of view and a few elongated grains from nucleation on the wall, or fragments stuck in the thickness for upward solidification experiments. It is worth noting that, based only on the last figure (Fig. 7h), it would not be possible to know if there was grain nucleation ahead of the columnar front or not. This remark shows clearly the great benefit of using in situ characterization for the

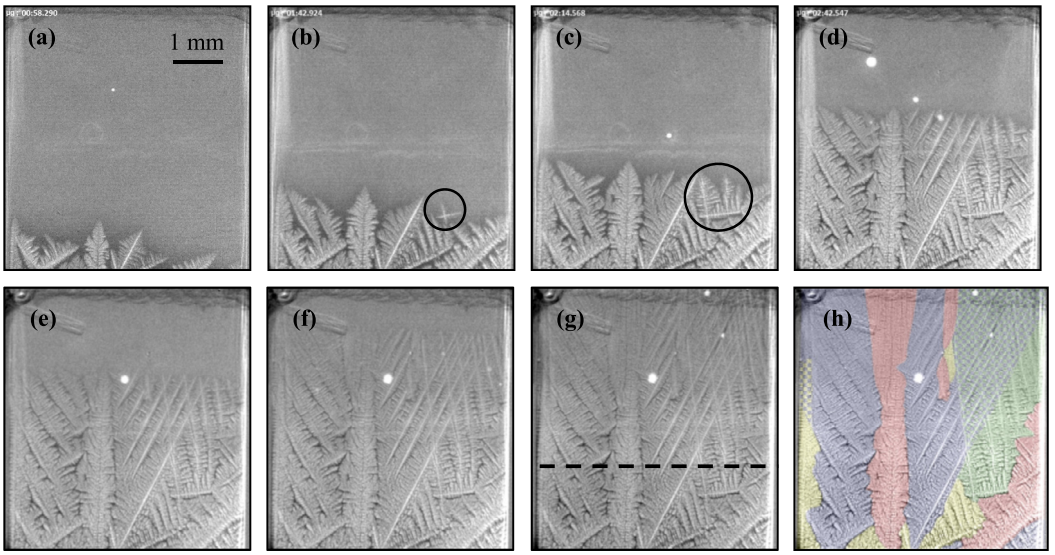

Fig. 7. Columnar solidification of Al–20wt%Cu in microgravity conditions, with a temperature gradient of about 150 K/cm between the two heaters and the three different cooling rates. Cooling rate of 0.15 K/s on both heaters, (a) $t = 317$ s, (b) $t = 360$ s, (c) $t = 382$ s. Change of cooling rate to 0.7 °C/s on both heaters, (d) $t = 418$ s. Natural cooling after switching off the power on both heaters, (e) $t = 422$ s, (f) $t = 426$ s, (g) $t = 433$ s after lift-off. (h) Final grain structure determined by drawing manually the boundaries of the different dendritic grains.

study of time-dependent phenomena. For the sake of completeness, it is also worth mentioning that a dark layer just ahead of the solidification front is visible, which is due to the solute (copper) rejection during the liquid-to-solid transformation.

4.3. Influence of convection on the solidification velocity

Based on the radiographs, it is possible to precisely measure the instantaneous growth rate as a function of time for each experiment (Fig. 8). In each case, the three successive growth rates are clearly visible and an average value can be deduced. The source of the uncertainties for all the experiments comes mainly from the limited spatial resolution during the measurement of the dendrite tip positions. The ground-based experiments were carried out after the flight with a new sample. According to the measurements, it was found that the values of the growth rates for the microgravity experiment (Fig. 8a) are closer to the values of the 1*g*-upward solidification (Fig. 8b) than to the values of the 1*g*-horizontal solidification (Fig. 8c). The same trend was observed during the breadboard tests carried out before the flight, with dendrites growing faster with the sample in horizontal position (20.5 µm/s) than in vertical position (18.6 µm/s).

The remarkable same values obtained for microgravity and 1*g*-upward experiments can be explained by the fact that natural convection in the latter case is dramatically minimized for several reasons. Firstly, solidification in the upward case is performed in both stable thermal and solutal conditions (hot zone placed above the cold zone and solute denser than the solvent), which minimize the occurrence of boundary layer convection similar to Al–Li beforehand described, in particular for high axial temperature gradient and high solidification velocities like in this experiment. Secondly, the high value of growth rates prevents the convective flow induced by residual transverse temperature gradient in this configuration similar to Al–Ni [36] and finally the high confinement in this sample (200 µm in thickness) strongly damped the fluid flow, if any.

The discrepancy between the growth rates of those experiments and the 1*g*-horizontal experiment is slight, but significant. Actually, for the sample solidification in 1*g*-horizontal position, the convective roll induced by thermal convection and/or the rejection of heavy solute within the thickness of the sample may be strong enough to modify the thermal or the solutal fields, then increasing the growth rates. Indeed, in the case of horizontal Bridgman growth, thermal convection occurs as soon as there is a temperature gradient along the sample (i.e. no threshold). Fortunately, if convection is not too strong and by neglecting solute concentration, it is possible to estimate the magnitude of convection effect by an Order of Magnitude Analysis (OMA) [43]. For thermal convection, J.-J. Favier defined a thermal convecto-diffusive parameter Δ_{th} as the ratio of the length of the solute boundary layer in convective regime to the length of the solute boundary layer in the pure diffusive regime. Δ_{th} can be expressed as a function of the Péclet number $Pe = eV/D$, of the Grashoff number $Gr = \beta_T g G e^4/\upsilon^2$ and the Schmidt number $Sc = \upsilon/D$:

$$\Delta_{\text{th}} = 4.5 Pe (GrSc)^{-1/3} \tag{3}$$

Using $e = 150$ µm, $D = 3 \cdot 10^{-9}$ m^2/s, $\nu = 4 \cdot 10^{-7}$ m^2/s, $\beta_T = 1.17 \cdot 10^{-4}$ K^{-1}, $g = 9.8$ m/s^2, $G = 15$ K/mm, $V_1 = 18.6$ µm/s, and $V_2 = 69$ µm/s, it is found that Δ_{th} is always larger than unity, which means that thermal convection is negligible compared to diffusion transport.

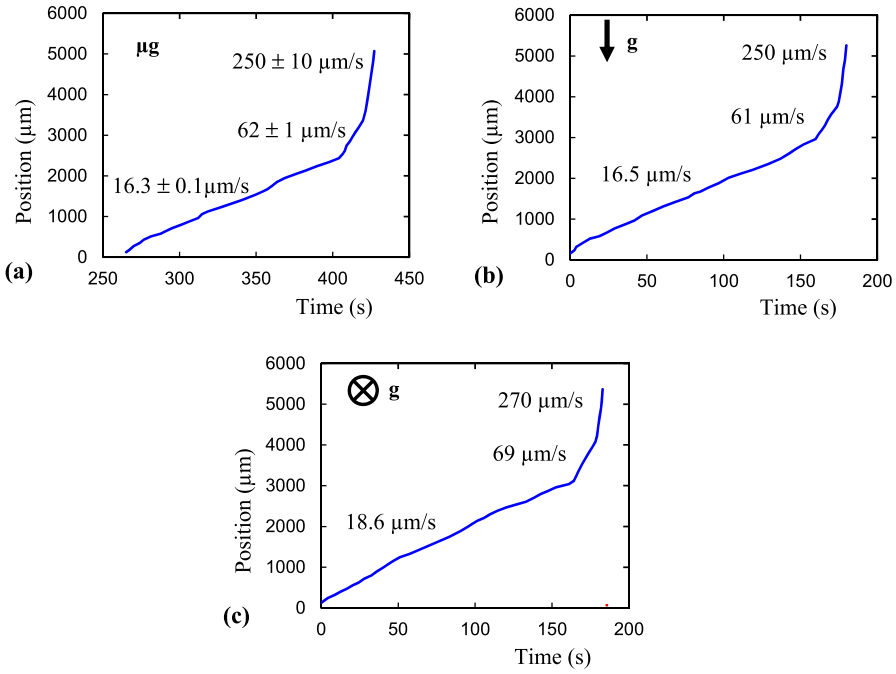

Fig. 8. Evolution of the solidification front velocity as a function of time during (a) the microgravity experiment, (b) the 1*g*-upward reference test and (c) the 1*g*-horizontal reference test.

On the other hand, the same OMA can be done for solutal convection [44]. In that case the expression of the convecto-diffusive parameter becomes:

$$\Delta_{sol} = 1.4Pe^{4/5}(1-k)^{-1/5}(Gr_S Sc)^{-1/5} \tag{4}$$

with Gr_S the solutal Grashoff number. Using $\beta_S = 0.73/\text{wt.\%}$, $C_0 = 20\text{wt.\%}$, $k = 0.14$, it was found that in our experiments, for both growth rates, Δ_{sol} is always lower than unity, which means that the solutal convection is not negligible and could interact with the columnar front and thus modify the growth rates.

5. Conclusions

It is now obvious that the earlier enthusiastic dreams regarding the potential of space manufacturing of innovative materials have given way to more realistic expectations. However, microgravity experimentation still offers a unique and efficient way for in-depth analysis of the pattern formation during directional solidification, in the limit of diffusive transport. Specifically, the models of solidification or numerical simulations (in particular the phase-field approach) need benchmark data to be validated, firstly in model situation, with diffusive transport conditions and then with convecto-diffusive transport to be able to describe and explain experimental results obtained in laboratories. It is obvious that the investigations of the influence of gravity, and more particularly natural convection, on solidification have to be further developed to achieve quantitative description of phenomena.

In this paper, a selection of our microgravity experiments was described. We left aside the recent outstanding experiments performed on the International Space Station on transparent alloys [17,18] or on Al–Si alloys [19,20]. Our intent was to show the slow but significant progress in our understanding of the influence of convection on the solidification microstructure. These studies enlightened key issues on the topic but also reported open questions, which gave us directions for future works. From the experimental point of view, the recent development of in situ characterization during microgravity solidification experiments opens new doors and will certainly give a new impetus to research in space.

Acknowledgements

This study was partly supported by the XRMON project (AO-2004-046; Grant no: 20288/06/NL/VJ) of the MAP program of the European Space Agency (ESA) and by the French National Space Agency (CNES; convention n^o 150515/00). The authors express their gratitude to Dr. Olivier Minster and Pr. Bernard Zappoli for their continuous support. The authors wish to acknowledge all the international partners who were involved in these projects: these scientific results could not have been achieved without their collaboration.

References

[1] J.A. Dantzig, M. Rappaz, Solidification, EPFL Press, Lausanne, Switzerland, 2009.
[2] H. Nguyen-Thi, et al., Investigation of gravity effects on solidification of binary alloys with in situ X-ray radiography on Earth and in microgravity environment, in: A. Meyer, I. Egry (Eds.), Proc. International Symposium on Physical Sciences in Space, Iop Publishing Ltd, Bristol, UK, 2011.
[3] A. Bogno, et al., Analysis by synchrotron X-ray radiography of convection effects on the dynamic evolution of the solid–liquid interface and on solute distribution during the initial transient of solidification, Acta Mater. 59 (2011) 4356–4365.
[4] G. Reinhart, et al., Investigation of columnar-equiaxed transition and equiaxed growth of aluminium based alloys by X-ray radiography, Mater. Sci. Eng. A 413–414 (2005) 384–388.
[5] G. Reinhart, et al., In-situ observation of transition from columnar to equiaxed growth in Al–3.5wt%Ni alloys by synchrotron radiography, in: Modeling of Casting, Welding and Advanced Solidification Processes XI, 2006, pp. 359–366.
[6] G. Reinhart, et al., In-situ and real-time analysis of the formation of strains and microstructure defects during solidification of Al–3.5wt. pct Ni alloys, Metall. Mater. Trans. A 39 (2008) 865–874.
[7] G. Reinhart, et al., In situ investigation of dendrite deformation during upward solidification of Al–7wt.%Si, JOM 66 (2014) 1408–1414.
[8] S. Akamatsu, H. Nguyen-Thi, In situ observation of solidification patterns in diffusive conditions, Acta Mater. 108 (2016) 325–346.
[9] M.E. Glicksman, et al., Dendritic growth velocities in microgravity, Phys. Rev. Lett. 73 (1994) 573.
[10] M.E. Glicksman, et al., Time-Dependent Behavior of Dendrites Under Diffusion-Controlled Conditions, Springer, Dordrecht, the Netherlands, 2001.
[11] J.C. LaCombe, et al., Nonconstant tip velocity in microgravity dendritic growth, Phys. Rev. Lett. 83 (1999) 2997–3000.
[12] M.B. Koss, et al., Dendritic growth tip velocities and radii of curvature in microgravity, Metall. Mater. Trans. A 30 (1999) 3177–3190.
[13] L.A. Tennenhouse, et al., Use of microgravity to interpret dendritic growth kinetics at small supercoolings, J. Cryst. Growth 174 (1997) 82–89.
[14] M.D. Dupouy, et al., Natural convection in directional dendritic solidification of metallic alloys – I. Macroscopic effects, Acta Metall. 37 (1989) 1143–1157.
[15] M.D. Dupouy, et al., Natural convective effects in directional dendritic solidification of binary metallic alloys: dendritic array morphology, J. Cryst. Growth 126 (1993) 480–492.
[16] M.D. Dupouy, et al., Natural convective effects in directional dendritic solidification of binary metallic alloys – dendritic array primary spacing, Acta Metall. Mater. 40 (1992) 1791–1801.
[17] F.L. Mota, et al., Initial transient behavior in directional solidification of a bulk transparent model alloy in a cylinder, Acta Mater. 85 (2015) 362–377.
[18] N. Bergeon, et al., Spatiotemporal dynamics of oscillatory cellular patterns in three-dimensional directional solidification, Phys. Rev. Lett. 110 (2013).
[19] D.R. Liu, et al., Simulation of directional solidification of refined Al–7wt.%Si alloys – comparison with benchmark microgravity experiments, Acta Mater. 93 (2015) 24–37.
[20] D.R. Liu, et al., Structures in directionally solidified Al–7wt.%Si alloys: benchmark experiments under microgravity, Acta Mater. 64 (2014) 253–265.
[21] S.H. Davis, Hydrodynamics interactions in directional solidification, J. Fluid Mech. 212 (1990) 241–262.
[22] G.B. McFadden, et al., Thermosolutal convection during directional solidification, Metall. Mater. Trans. A 15 (1984) 2125–2137.
[23] M.E. Glicksman, et al., Interaction of flows with the crystal-melt interface, Annu. Rev. Fluid Mech. 18 (1986) 307.
[24] B. Drevet, et al., Cellular and dendritic solidification of Al–Li alloys during the D2-mission, Adv. Space Res. 16 (1995) 173–176.
[25] B. Drevet, et al., Solidification of aluminum–lithium alloys near the cell/dendrite transition – influence of solutal convection, J. Cryst. Growth 218 (2000) 419–433.
[26] H. Nguyen Thi, et al., Influence of thermosolutal convection on the solidification front during upwards solidification, J. Fluid Mech. 204 (1989) 581–597.
[27] J.P. Garandet, et al., Segregation phenomena in crystal growth from the melt, in: D.T.J. Hurle (Ed.), Handbook of Crystal Growth, Elsevier Science B.V., North-Holland, 1994, p. 661.
[28] H. Nguyen Thi, et al., Cellular arrays during upward solidification of Pb–30wt%Tl alloys, J. Phys. France 51 (1990) 625–637.
[29] B. Billia, et al., Statistical analysis of the disorder of two-dimensional cellular arrays in directional solidification, Metall. Mater. Trans. A 22 (1991) 3041–3050.
[30] B. Billia, et al., Extrinsic effects in the dynamics and selection of cellular arrays, J. Thermophys. Heat Transf. 8 (1994) 113–118.
[31] C. Weiss, N. Bergeon, N. Mangelinck-Noël, B. Billia, Cellular pattern dynamics on a concave interface in three-dimensional alloy solidification, Phys. Rev. E 79 (2009) 011605.
[32] J.D. Hunt, S.Z. Lu, Numerical modeling of cellular dendritic array growth: spacing and structure predictions, Metall. Mater. Trans. A 27 (1996) 611–623.
[33] H. Nguyen Thi, et al., Preparation of the initial solid–liquid interface and melt in directional solidification, J. Cryst. Growth 253 (2003) 539–548.
[34] M.H. Burden, et al., Macroscopic stability of a planar, cellular or dendritic interface during directional freezing, J. Cryst. Growth 20 (1973) 121–124.
[35] H. Nguyen Thi, et al., In situ and real-time analysis of TGZM phenomena by synchrotron X-ray radiography, J. Cryst. Growth 310 (2008) 2906–2914.
[36] H. Nguyen Thi, et al., Directional solidification of Al–1.5wt%Ni alloys under diffusion transport in space and fluid flow localisation on Earth, J. Cryst. Growth 281 (2005) 654–668.
[37] A. Bogno, et al., In situ analysis of the influence of convection during the initial transient of planar solidification, J. Cryst. Growth 318 (2011) 1134–1138.
[38] M. Ben Amar, B. Moussalam, Absence of selection in directional solidification, Phys. Rev. Lett. 60 (1988) 317.
[39] A. Ludwig, et al., Advanced solidification studies on transparent alloy systems: a new European solidification insert for material science glovebox on board the international space station, JOM 64 (2012) 1097–1101.
[40] H. Nguyen-Thi, et al., On the interest of synchrotron X-ray imaging for the study of solidification in metallic alloys, C. R. Physique 13 (2012) 237–245.
[41] S. Akamatsu, H. Nguyen-Thi, In situ observation of solidification patterns in diffusive conditions, Acta Mater. 108 (2016) 325.
[42] H. Nguyen-Thi, et al., XRMON-GF: a novel facility for solidification of metallic alloys with in situ and time-resolved X-ray radiographic characterization in microgravity conditions, J. Cryst. Growth 374 (2013) 23–30.
[43] J.J. Favier, Macrosegregation. 1. Unified analysis during non-steady state solidification, Acta Metall. 29 (1981) 197–204.
[44] F.Z. Haddad, et al., Solidification in Bridgman configuration with solutally induced flow, J. Cryst. Growth 230 (2001) 188–194.